Blind-prediction: estimating the consequences of vented hydrogen deflagrations for inhomogeneous mixtures in 20-foot ISO containers

Trygve Skjold [a], Helene Hisken [a], Laurence Bernard [a], Lorenzo Mauri [a], Gordon Atanga [a], Sunil Lakshmipathy [a], Melodia Lucas Pérez [a], Marco Carcassi [b], Martino Schiavetti [b], Vendra Chandra Madhav Rao [c], Anubhav Sinha [c], Ilias C. Tolias [d], Stella G. Giannissi [d], Alexandros G. Venetsanos [d], James R. Stewart [e], Olav Roald Hansen [f], Chenthil Kumar [g], Laurent Krumenacker [h], Florian Laviron [i], Romain Jambut [i] & Asmund Huser [j]

E-mail: *trygve@gexcon.com*

[a] Gexcon, Fantoftvegen 38, 5072 Bergen, Norway
[b] University of Pisa, Largo Lucio Lazzarino 2, 56122 Pisa, Italy
[c] Warwick FIRE, School of Engineering, University of Warwick, Coventry, UK
[d] Environmental Research Laboratory, National Center for Scientific Research Demokritos, Agia Paraskevi, 15310, Greece
[e] HSE, Harpur Hill, Buxton, Derbyshire, SK17 9JN, UK
[f] Lloyd's Register, Kokstadflaten 35, 5863 Bergen, Norway
[g] Fluidyn, 146 Ring Road, Bangalore 560102, India
[h] Fluidyn, 7 Blvd. de la Libération, 93200 Saint-Denis, France
[i] DNV GL, 69 Rue Chevaleret, 75013 Paris, France
[j] DNV GL, Veritasveien 1, 1337 Høvik, Norway

Abstract

This paper summarises the results from a blind-prediction benchmark study for models used for estimating the consequences of vented hydrogen deflagrations. The work was part of the HySEA project that received funding from the Fuel Cells and Hydrogen Joint Undertaking (FCH JU) under grant agreement no. 671461. The first blind-prediction benchmark exercise in the HySEA project focused on vented explosions with homogeneous hydrogen-air mixtures in 20-foot ISO containers. The scenarios selected for the second blind-prediction study focused on vented deflagrations in inhomogeneous hydrogen-air mixtures resulting from continuous stratification of hydrogen during vertical jet releases inside 20-foot ISO containers. The deflagrations were vented through commercial vent panels located on the roof of the containers.

The test program included two configurations and four experiments, i.e. two repeated tests for each scenario. The paper compares experimental results and model predictions and discusses the implications of the results for safety related to hydrogen applications. Several modellers predicted the stratification of hydrogen inside the container during the release phase with reasonable accuracy. However, there is significant spread in the model predictions, especially for the maximum reduced explosion pressure, including predictions from different modellers using the same model system. The results from the blind-prediction benchmark studies performed as part of the HySEA project constitute a strong incentive for developers to improve their models, implement automated procedures and update guidelines for users of the models.

Keywords: *blind-prediction, vented deflagration, hydrogen safety, inhomogeneous mixtures*

1. Introduction

1.1 The HySEA project

This paper presents results from the second blind-prediction study in the HySEA project. Fires and explosions represent a significant hazard for hydrogen installations, and specific measures are generally required for reducing the risk to a tolerable level (Skjold *et al.*, 2017; Skjold *et al.*, 2018a). To this end, it is important to validate and document the performance of the models used for assessing the potential consequences of relevant accident scenarios. Explosion venting is a frequently used measure for reducing the consequences of deflagrations in confined systems. The main objective of the project *Improving Hydrogen Safety for Energy Applications through pre-normative research on vented deflagrations* (HySEA) was to develop recommendations for improved international standards for the design of explosion venting devices, such as EN 14994 (2007) and NFPA 68 (2018). The members of the HySEA consortium were Gexcon (coordinator), University of Warwick (UWAR), University of Pisa (UNIPI), Fike Europe, Impetus Afea and Hefei University of Technology (HFUT).

1.2 Previous work

Vented hydrogen deflagrations have been extensively studied in the past, but primarily for initially quiescent mixtures ignited to deflagration in empty enclosures (Razus & Krause, 2001; Bauwens *et al.*, 2011; Bauwens *et al.*, 2012; Sustek & Janovsky, 2013; Bauwens & Dorofeev, 2014; Molkov & Bragin, 2015). Sommersel *et al.* (2008, 2017) investigated the effect of initial turbulence and congestion for vented hydrogen explosions in a 20-foot ISO container. Several blind-prediction or benchmark studies have been conducted for hydrogen in the past (e.g. Baraldi *et al.* 2010; Baraldi *et al.*, 2017; García *et al.*, 2010; Makarov *et al.*, 2009). Baraldi *et al.* (2010) highlighted the need for blind-prediction benchmark studies for proper evaluation of the predictive capabilities of consequence models. The results from the first blind-prediction benchmark study in the HySEA project, that focused on vented deflagrations in homogeneous lean hydrogen-air mixtures, revealed significant spread in the model predictions (Skjold *et al.*, 2018b), for computational fluid dynamics (CFD) codes as well as engineering models (EMs) based on empirical correlations.

1.3 The second HySEA blind-prediction benchmark study

The experimental program in the HySEA project included 66 vented hydrogen deflagration experiments performed in 20-foot shipping containers: 42 tests with initially homogeneous and quiescent mixtures, and 24 tests with inhomogeneous mixtures (Skjold, 2018; Skjold *et al.*, 2018c). The total number of tests was 72, which included five unignited dispersion tests and one failed test. The scenarios selected for the second HySEA blind-prediction benchmark exercise involved continuous stratification of hydrogen and subsequent ignition to deflagration and explosion venting through commercial vent panels. The HySEA consortium invited researchers and engineers to submit model predictions prior to the completion of the actual experiments. The call for model predictions was published on the HySEA website and distributed by e-mail. University of Pisa collected the model predictions. The submission deadline was 30 November 2017. Three commissioning tests without ignition were completed in October 2017 (Table 1), but the results were not communicated to the modellers. Seven individuals/groups submitted predictions obtained with CFD tools, and one group submitted predictions from various engineering models. Although all model predictions were submitted prior to the vented deflagration experiments, one prediction was resubmitted after the first experiment had been completed because the simulation was still running when the deadline expired. It was clear from the results that the resubmitted data were from the same simulation as previously submitted.

2 Experiments

This chapter describes the test rig, the measurement system, and the experimental procedure.

2.1 Test rig

Gexcon performed the experiments at the remote test site on the island of Sotra outside Bergen. The experimental rig used for the HySEA experiments consisted of a standard 20-foot ISO container fitted with a steel frame on the floor. The purpose of the steel frame was to support obstacles and instrumentation inside the container, and to fix the container to a solid foundation. Figure 1 shows one of the twelve 20-foot ISO containers used in the experimental campaign (left) and the interior of a container ready for testing (right). The red arrow indicates the position and direction of the jet releases. Figure 2 shows the steel frame (the white structure on the floor in Figure 1) placed on top of the foundation during construction of the test rig.

Figure 1: 20-foot ISO container (left) and the interior of the container (right).

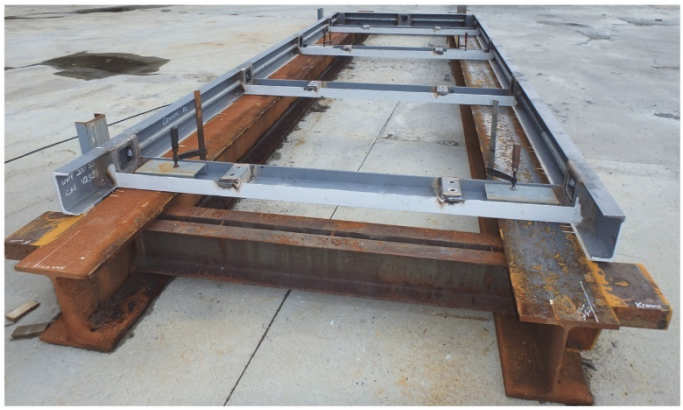

Figure 2: The steel frame (grey) on top of the foundation.

Figure 3 shows the overall dimensions of the steel frame and the position of the eight bolts used for fixing the frame to the foundation. The foundation was made from two 360-mm H-beams, which implies that the bottom of the container was positioned 0.36 m above ground level during testing. The containers were fixed to the foundation by four bolts along each side of the container, passing through the steel frame. The steel frame was constructed from U-beams (UNP 200, Figure 3). The U-beams positioned along the back wall and both side-walls of the container had the flat side facing the container walls to minimise flame acceleration in the gap between the frame and the corrugated wall.

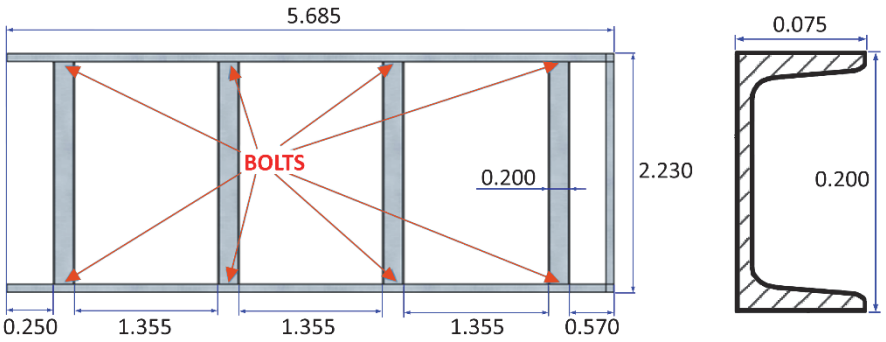

Figure 3: Dimensions of steel frame (left) and cross-section of U-beam (right).

Figure 4 summarises the overall dimensions of the containers. The inner dimensions were 5.87 m × 2.35 m × 2.39 m, for a total volume of about 33 m^2. The floor inside the containers was covered with plywood, and the walls and the roof were made of corrugated steel plates. The level of the floor was about 0.50 m above ground level during testing. The depth of the corrugations in the walls was 35 mm, one 'period' of corrugation 280 mm, and plate thickness 2.0 mm. The depth of the corrugations on the roof was 16 mm, one 'period' of corrugation 210 mm, the plate thickness 2.0 mm.

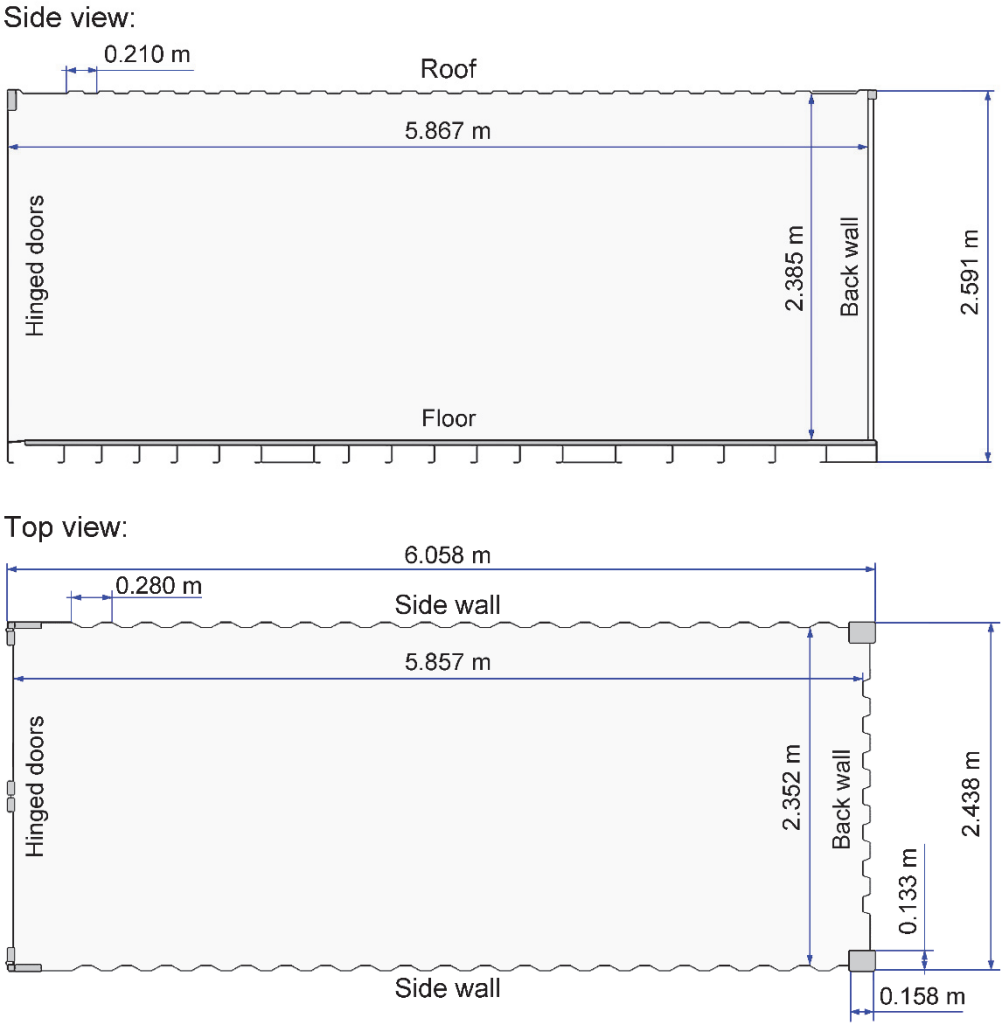

Figure 4: Overall dimensions (m) of a 20-foot ISO container.

The corrugated plate on the roof of the containers was replaced with a tailor-made steel frame that supported the vent panels. This frame was made from 100 mm x 100 mm square pipes and a 100 mm x 80 mm rectangular pipe along the centre. The frame was connected to the frame inside the container with chains (Figure 1). Six of the eight 1.0 m × 1.0 m openings were covered with single-sheet bulged vent panels with vent area A_v 1.0 m^2 and nominal static opening pressure P_{stat} 100 mbar (specified opening pressure 75-125 mbar). The remaining openings in the roof were closed with blind flanges. Figure 5 illustrates the position of the vent panels, ignition source, pipe rack and jet release. The dimensions of the two blocked openings towards the container doors were 1.0 m × 0.56 m. Figure 6 shows a container with six panels (A_v = 6.0 m^2) before and after a test (container doors on the left).

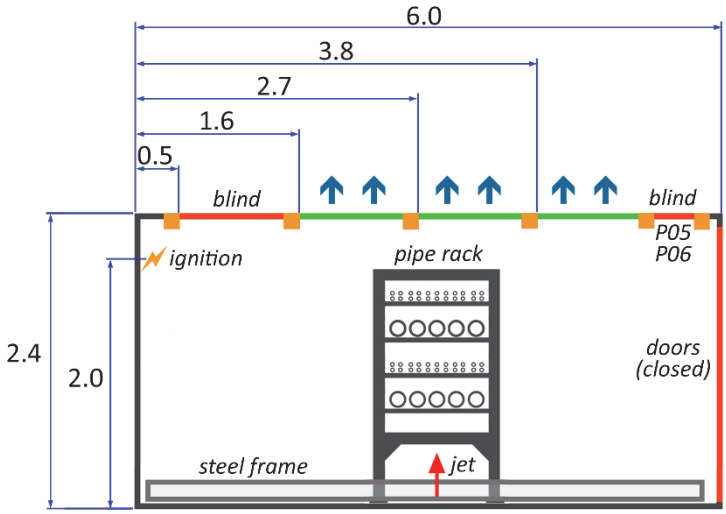

Figure 5: Schematic illustration of container and vent openings.

Figure 6: Container with six commercial vent panels before and after a test.

Figure 7 shows the pipe rack obstacle. The obstacle consisted of a steel frame made from 100 mm × 100 mm square pipes, and four layers of round pipes: two shelves with five pipes each, pipe diameter 104 mm, 200 mm spacing, and fixed with U-bolts, and two shelves with 22 pipes

in two layers, pipe diameter 20 mm, 100 mm spacing in horizontal direction, 33 mm spacing in vertical direction, and fixed with standard support clamps for hydraulic pipes. All pipes were 1200 mm long. The shelves for fixing the pipes were made from 50 mm × 50 mm angle steel, with heights above the floor of the container of 600, 800, 1100 and 1400 mm. The pipe rack was fixed with brackets to the frame inside the container. Figure 1 (right) shows the pipe rack mounted in the centre position, denoted configuration P2. Three one-inch pipes (outer diameter about 34 mm) prevented the upper part of the container from bulging out. The centre of these pipes was about 80 mm below the frame that supports the vent panels.

Figure 7: Pipe rack (left) and brackets fixed to frame inside container (right).

2.2 Measurement system

Figure 8 summarises the measurement system. Four NI CompactDAQ type 9215 (BNC) data acquisition modules from National Instruments, mounted in a cDAQ-9188XT chassis located in the instrumentation bunker, recorded the pressure and deflection measurements at a sampling frequency of 100 kHz. A separate National Instruments NI-9201 data logger was used for the concentration measurements. The explosion events were recorded with two Edgertronic SC1 high-speed video cameras and one regular JVC GZ-RX515BE video camera.

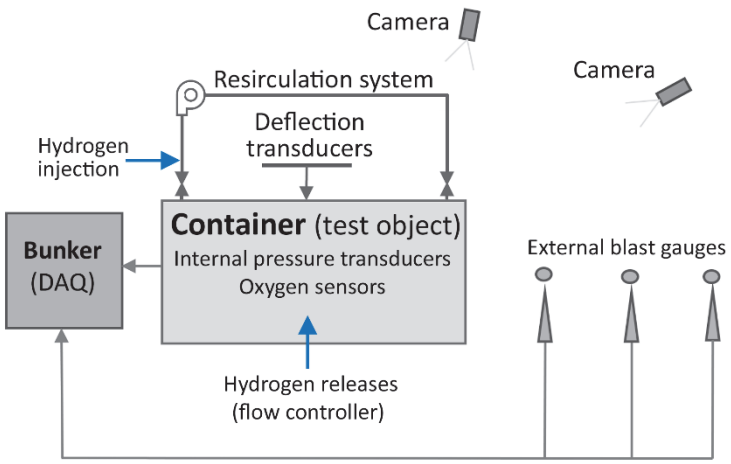

Figure 8: Schematic overview of the measurement system.

Figure 9 illustrates the position of the vertical jet release (R01) and the eight internal pressure sensors: P01-P02 (Kistler 701A), P03-P04 (Kistler 701A), P05-P06 (Kistler 7261) and P07-P08 (Kistler 7031), all used with Kistler 5073A charge amplifiers. The sensors P01-P02 and P07-P08 were positioned on the horizontal surface of the U-beams along the side walls of the container, in the same distances from the back wall as the bolts holding the frame (Figure 3), 85 mm from the side wall, and 200 mm above the floor of the container. Sensors P03 and P04 were positioned at the vertical surface facing the container doors, about 100 mm above the floor. Sensors P05 and P06 were positioned in the blind flanges (ceiling) near the doors. Due to the symmetry of the geometry, each pair of sensors (P01 & P02, P03 & P04, etc.) should in principle measure identical pressures.

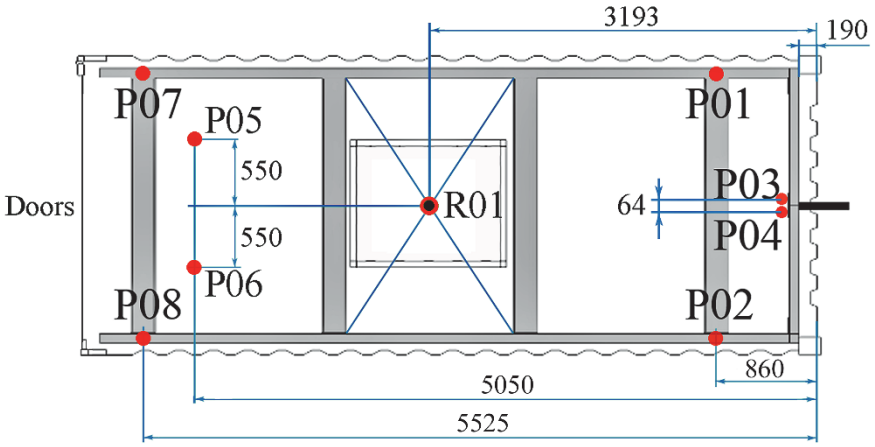

Figure 9: Approximate positions (mm) for the internal pressure sensors P01-P08.

Three Kistler 4043A2 piezoresistive pressure gauges with Kistler 4601 amplifiers measured the far-field blast pressures P09-P11 outside the container, 5, 10 and 15 m from the container doors, and about 1.65 m above the ground. Two Acuity AR700-50 Laser displacement sensors, operated at 10 kHz, measured the structural displacement of the container walls. A digital thermal mass flow meter and controller from Brooks Instrument (Model SLA5853S2EAB2C2A1) controlled the flow rate of hydrogen into the container. Figure 10 illustrates the position of the concentration measurements in a vertical cross-section of the container.

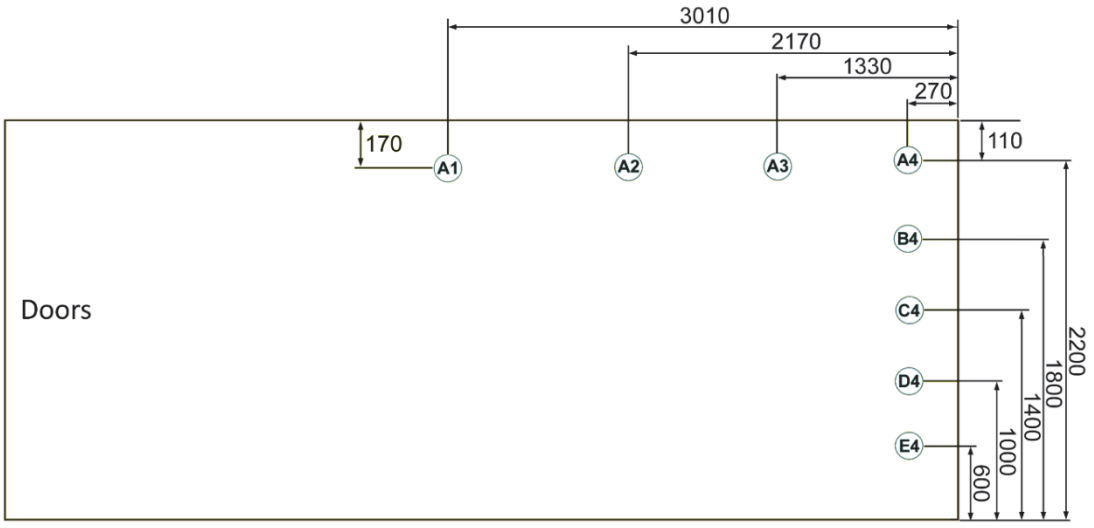

Figure 10: Positions (mm) for the concentration measurements.

Figure 11 shows the front side of the container with the five sampling tubes for the Servomex Xendos 2223 oxygen transmitter/analyser in positions A4'-E4', and the opposite side with eight low-cost oxygen sensors from Teledyne instruments (oxygen sensor class R-22A) in positions A1-E4. All measurements were taken close to the side walls. The symmetric location of the vertical row of probes (A4, B4, etc.) and sampling tubes (A4', B4', etc.) near the back wall implies that the continuous and intermittent concentration measurements should measure more or less the same concentration profile for the stratified mixture inside the container. Figure 12 shows the pipe used for the vertical jet release.

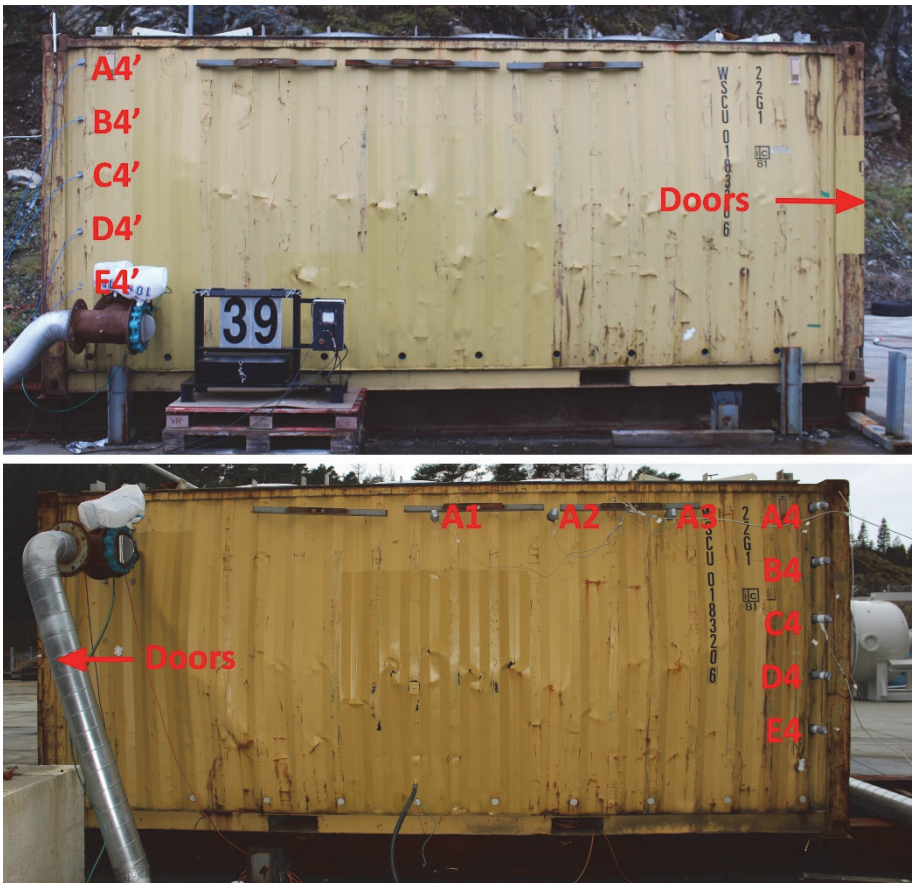

Figure 11: The tubes for the Servomex analyser (above) and the low-cost oxygen sensors (below).

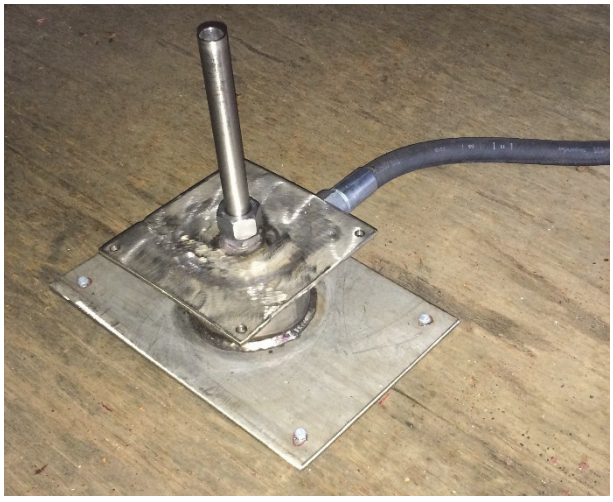

Figure 12: Pipe used for vertical jet release.

The pipe for the jet release had outer and inner diameters 22 mm and 18 mm, respectively. The release point was positioned along the centre line of the container, about 3.2 m from the back wall, 0.30 m above the floor, pointing upwards. A horizontal plate, with dimensions 0.2 m × 0.2 m, was located about 0.2 m below the release point. This plate was used for tests with diffusive releases (not part of the blind-prediction study). Measurements with thermocouples located in the jet, immediately downstream of the release point, indicated that the release temperature was within 1-3 ºC of the ambient temperature.

Figure 8 illustrates the recirculation system, that consisted of 4-inch flexible air ducts, a fan, and two remotely operated butterfly valves (Figure 11) for isolating the ducts and fan from the container prior to ignition. This system was not used for the tests with inhomogeneous mixtures, but it was installed as a precautionary measure in the event it would be necessary to empty flammable mixture from a container in the event of unsuccessful ignition.

2.3 Experimental procedure

Table 1 summarises the test matrix, including three commissioning tests without ignition. Figure 5 shows the location of the vent openings, the jet release and the pipe rack. Tests 57 and 59 were repeated tests with frame only (FO), i.e. without the pipe rack present. Tests 60 and 61 were repeated tests with the pipe rack in centre position (P2). The asterisks for test numbers 57, 60 and 61 indicate that the test container had to be replaced after these tests due to severe structural deformation.

Table 1: Test matrix for the second HySEA blind-prediction benchmark exercise.

Test	Date	A_v (m^2)	Ign.	C_n (vol.%)	Geometry	T_{amb} (ºC)
T39	19.10.2017	–	–	21	P2	9
T42	23.10.2017				FO	13
T43	23.10.2017					15
T57*	30.11.2017	6.0	BU		FO	-3
T59	05.01.2017					-3
T60*	08.01.2017				P2	3
T61*	09.01.2017					0

Table 2 summarises selected results from the four ignited tests: the maximum reduced explosion pressures P_m and the maximum pressure impulse I_m recorded by the internal pressure sensors P01-P08, the maximum deflection D_m and permanent deformation D_p measured with lasers approximately 14 cm above the centre of the side walls (1.9 m above the ground), the time t_{stat} and internal pressure P_{stat} when the panels start to open, and the times t_{45}, t_{90} and t_{180} relative to t_{stat} when the panels were 45º, 90º and 180º open, respectively. The opening times for the panels were estimated from high-speed video recordings.

Table 2: Selected results from the four ignited tests in the blind-prediction benchmark exercise.

Test	P_m (bar)	I_m (bar-ms)	D_m (m)	D_p (m)	t_{stat} (s)	$P_{stat, P7}$ (bar)	t_{45} (s)	t_{90} (s)	t_{180} (s)
T57*	0.343	7.9	0.180	0.042	0.082	0.112-0.126	0.022	0.035	0.059
T59	0.343	8.0	0.196	0.030	0.083	0.101-0.117	0.026	0.038	0.061
T60*	0.370	9.6	0.196	0.064	0.096	0.102-0.117	0.025	0.036	0.058
T61*	0.676	11.6	0.432	0.263	0.076	0.097-0.110	0.025	0.034	0.050

Gaseous hydrogen was released into the container at a constant flow rate of 56 Nm^3 hr^{-1} (equivalent to 0.00133 kg s^{-1}) through a vertical pipe with inner diameter 18 mm. The open end of the pipe was located 0.3 m above the floor of the container. The duration of the release was 7.5 minutes (450 s). Distributed openings in the side walls allowed excess gas to escape: 20 holes, 10 on each side of the container, 51 mm (2 inches) in diameter, and 100 mm above the floor. Assuming only air escaped from the container, the nominal (average) fuel concentration C_n at the time of ignition should be 21 vol.% (Table 1). However, some fuel may have escaped, either through small openings in the ceiling or through the openings in the side walls close to the floor.

Hydrogen concentrations were measured near the corners of the container, in the opposite end from the container doors (Figure 10 and Figure 11), during the release and up to the time of ignition. The ignition source, an inductive spark with energy release about 1 mJ, was activated about 8 minutes (480 s) after the release started (i.e. 30 s after the release ended). The spark plug was located at the back wall, about 2.0 m above the floor (denoted BU in Table 1). The explosions were vented through six 1.0 m × 1.0 m vent openings on the roof of the container (Figure 5), covered with single-sheet bulged vent panels: A_v = 1.0 m^2, P_{stat} = 0.10 ± 0.25 bar, specific weight 6.8 kg m^{-2}. The container doors were closed during the tests.

3 Consequence models

3.2 Empirical and phenomenological models

Table 3 summarises the empirical and phenomenological engineering models (EMs) used for model predictions. This category of models will typically rely on theoretical expressions and/or empirical correlations, and the calculation time for a given scenario is very short. The results for the modified External Cloud Model (ECM-II) were submitted after the tests had been performed.

Table 3: Empirical and phenomenological engineering models.

Modeller	EM	Reference
M-8	EN 14994	EN 14994 (2007)
	NFPA-68	NFPA-68 (2013)
	FM Global	Bauwens *et al.* (2012)
	Molkov	Molkov & Bragin (2015)
	External Cloud Model (ECM-I)	Sinha *et al.* (2018ab)
	External Cloud Model (ECM-II)	Sinha & Wen (2018)

3.1 CFD tools

Table 4 summarises the CFD-based consequence models used for model predictions. The calculation time for a given scenario can vary from less than an hour to several days. For the sake of brevity, the model descriptions focus on version numbers, grid resolution, CFL numbers used, etc. For technical details, please refer to the respective user manuals and cited publications.

Table 4: Overview of the CFD tools used in the blind-prediction benchmark study.

Modeller	Model description
M-1	***FLACS v10.6 r3*** (Gexcon, 2018) Dispersion simulations with 0.10 m grid cells, local refinement near leak (0.016 m), and variable CFL conditions. The explosion simulations used 0.10 m uniform grid with initial conditions from dispersion simulation after 480 s. Pressure relief panels modelled as pop-out panels with activation pressure 0.10 bar. In the original submission (M1a), the monitor points for the dispersion simulations were positioned relative to the ground and not the floor of the container, i.e. about 0.5 m too low. This is corrected for prediction M1b.
M-2	***Fluidyn*** Minimum grid resolution 0.007 m (FO) and 0.00092 m (P2), k-epsilon turbulence model. Computational time steps 0.1 s for the release scenarios and 0.00005 s for the explosion scenarios. Modified BML combustion model with single step reactions. Symmetry plane.
M-3	***OpenFOAM*** Large eddy simulation (LES), flame area wrinkling combustion model and laminar burning velocity correlation. Hydrogen assumed ideal gas.
M-4	***ADREA-HF*** (Venetsanos *et al.,* 2010) Symmetry on y-axis, standard k-ε turbulence model with additional buoyancy terms, ideal gas assumption. Dispersion: 2 cells were used to discretise hydrogen inlet (minimum cells size 0.009 m), total number of cells 664 576 and 912 789 for the FO and P2 case, respectively. CFL = 40 (time step = 0.015 s during release). Combustion: Approximately uniform grid (0.05 m cell size) inside the enclosure for the FO case, refinement (0.03 m) in non-vertical directions at obstacles area in the P2 case. Total number of cells 1 758 120 and 1 919 580 respectively. Combustion model based on the Yakhot equation for turbulent burning velocity and modifications to account for flame instabilities. All vents assumed to open instantaneously and simultaneously when the overpressure at the position of the middle pair of panels reached 0.1 bar.
M-5	***FLACS v10.6 r3*** (Gexcon, 2018) Release scenario modelled with compressible solver and CFLV of 2 for efficient calculations. Base grid for dispersion 0.20 m in horizontal and 0.10 m in vertical direction, automatic refinement around leak (0.018 m) and 0.05 m vertical in lower part of chamber. Explosion simulations with 0.10 m grid resolution inside container and outside vent, and 0.20 m outside container. Sensitivity study on panel weight and effective opening area indicated limited impact on simulation results.
M-6	***FLACS v10.6 r3*** (Gexcon, 2018) Dispersion simulations with 0.07 m grid cells and local refinement near leak (0.045 m), and 0.06 (a), 0.07 (b), 0.08 (c) and 0.10 m (d) grid cells for explosion simulations. Boundary conditions: NOZZLE for dispersion cases and PLANE WAVE for explosion cases. Used density of hydrogen at 15 °C to convert between mass and volume flow.
M-7	***FLACS 10.2*** (Gexcon, 2018) Grid resolution 0.10 m (a) for dispersion simulations, and conversion of the resulting cloud to coarser meshes (b-d) using the rd-file utility in FLACS. Grid resolution 0.10 (a), 0.15 (b), 0.20 (c) and 0.30 m (d) for explosion simulations. Dispersion simulations used CFLV = 5 and CFLC = 125, and explosion simulations used CFLV = 0.5 and CFLC = 5.

4 Experimental results

4.1 Release rates

Figure 13 summarises the flow rates measured with the digital thermal mass flow meter and controller. All measurements indicate a near constant flow rate of 56 Nm^3 hr^{-1} for 450 s. However, it is not clear whether the deviation from zero (about 3 Nm^3 hr^{-1}) in the initial flow for tests 57 and 59 imply that the actual flow rates for these tests were closer to 53 Nm^3 hr^{-1}, especially since the curve for test 59 returns to zero while the curve for test 57 do not. The concentration profiles measured at 480 s (Figure 17) show consistently lower concentrations for tests 57 and 59 relative to tests 42 and 43, indicating reduced flow rates and/or leakage.

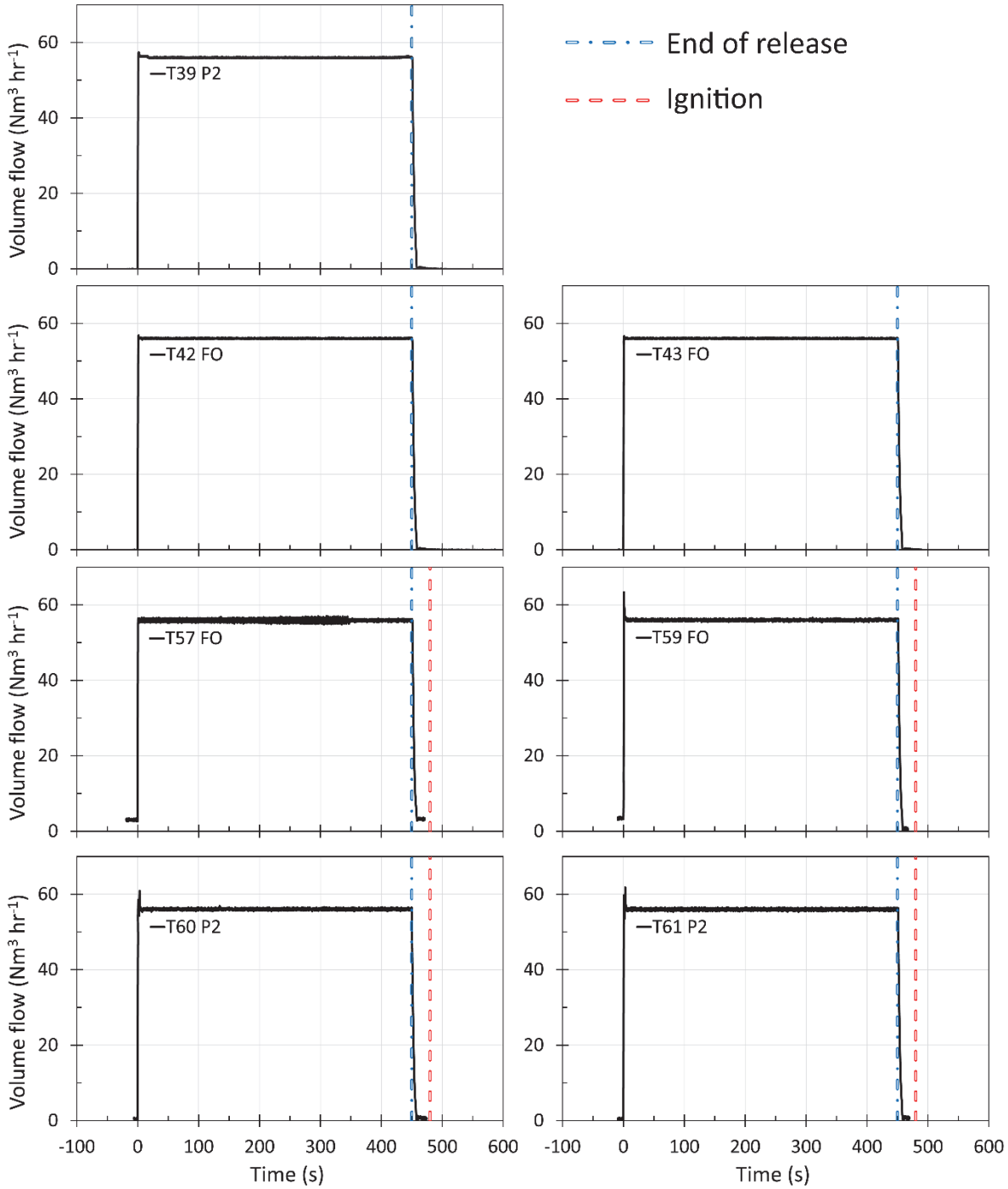

Figure 13: Measured flow rates.

4.2 Dispersion and stratification

Figure 14 summarises the results from two unignited tests: T42 (FO) and T39 (P2). The vertical dash-dotted lines at 450 s indicate the end of the releases. There is reasonable agreement between the results obtained with the low-cost oxygen sensors (continuous lines) and the intermittent measurements with the Servomex analyser (points). The results demonstrate clear stratification inside the container, with maximum hydrogen concentrations around 27 vol.%. The pipe rack (P2) has limited influence on the distribution of hydrogen inside the enclosure.

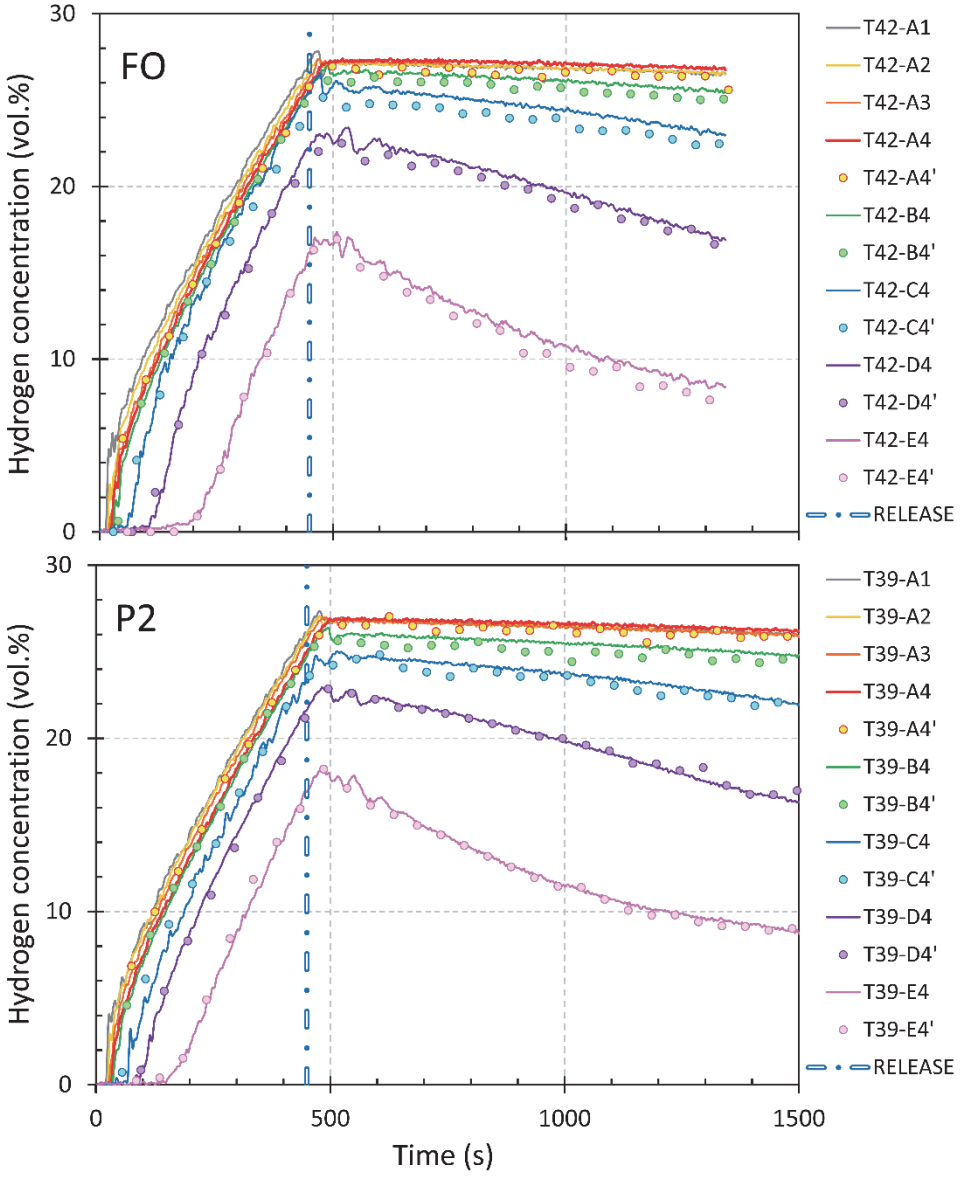

Figure 14: Hydrogen concentrations for unignited tests with frame only (FO) and pipe rack (P2).

Figure 15 documents the repeatability of the dispersion process for ignited and unignited releases. The concentrations obtained for ignited tests 57, 59 and 60 are somewhat lower than the corresponding unignited tests 42 and 39. This indicates that the flow rate may have been less than 56 $Nm^3\ hr^{-1}$ for tests 57 and 59 (Figure 13), and/or that some fuel may have escaped through the roof. Since all measurements indicate mixtures on the lean side, i.e. below about 30 vol.% hydrogen in air, a lower concentration at the time of ignition will typically result in lower maximum reduced explosion pressures in the vented deflagrations.

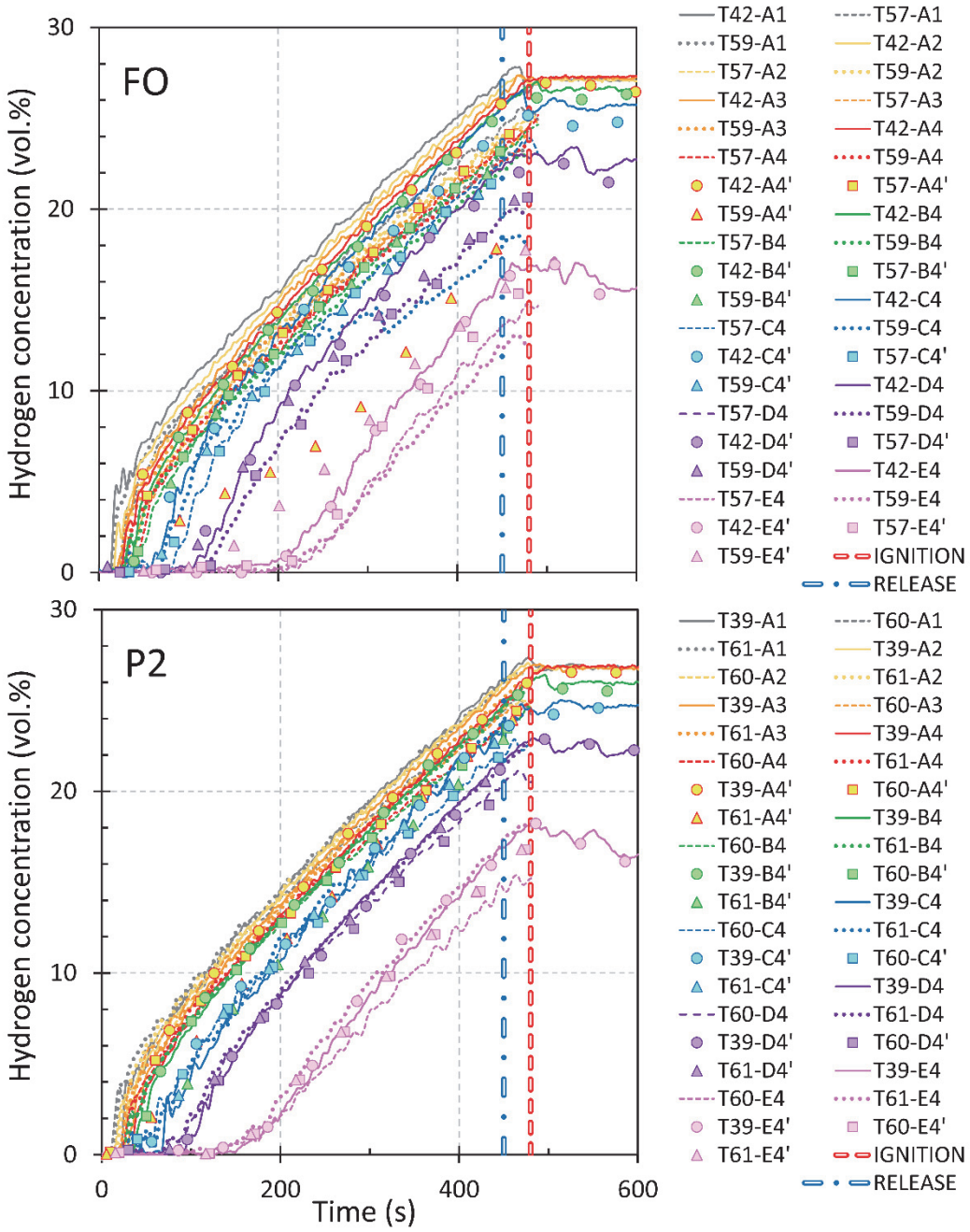

Figure 15: Hydrogen concentrations for unignited and ignited tests for both scenarios (FO and P2).

4.3 Pressure development

Figure 16 shows smoothed pressure-time histories from the four ignited tests. Skjold *et al.* (2018c) describe the data processing and filtering in detail. The vertical dash-dotted lines indicate the degree of opening for the hinged vent panels. Figure 17 shows selected frames from test 61: *a)* when the vent panels start to open (t_{stat}), *b-e)* when the panels are approximately 45°, 90°, 180° and 270° open, and after the test *f)*. For simplicity, and because of significant drift in some of the signals, the plots show only one pressure-time curve for each pair of symmetrically placed pressure sensors (Figure 9). Overall, the overpressures increase somewhat with the introduction of the pipe rack (P2). The highest pressures are obtained for pressure transducer P7 in test 61. As shown in Figure 15, this is the only ignited test where the measured hydrogen concentrations were at the same level as in the unignited tests.

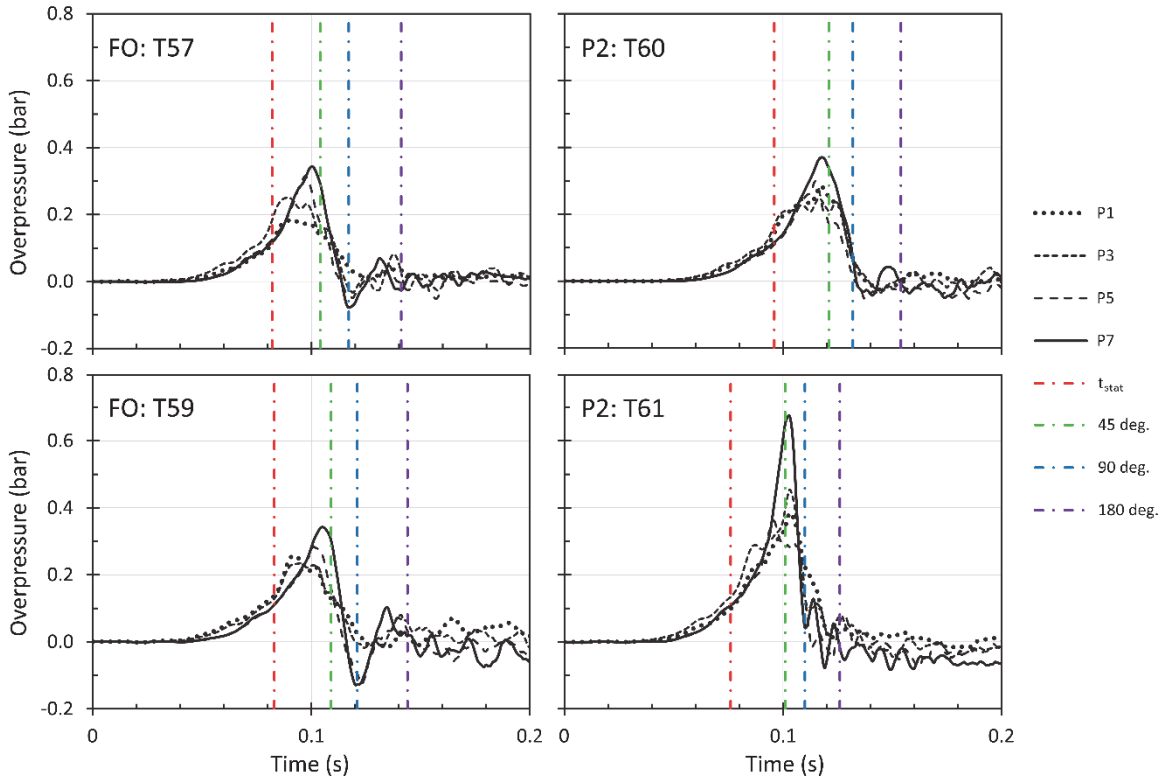

Figure 16: Experimental pressure-time histories.

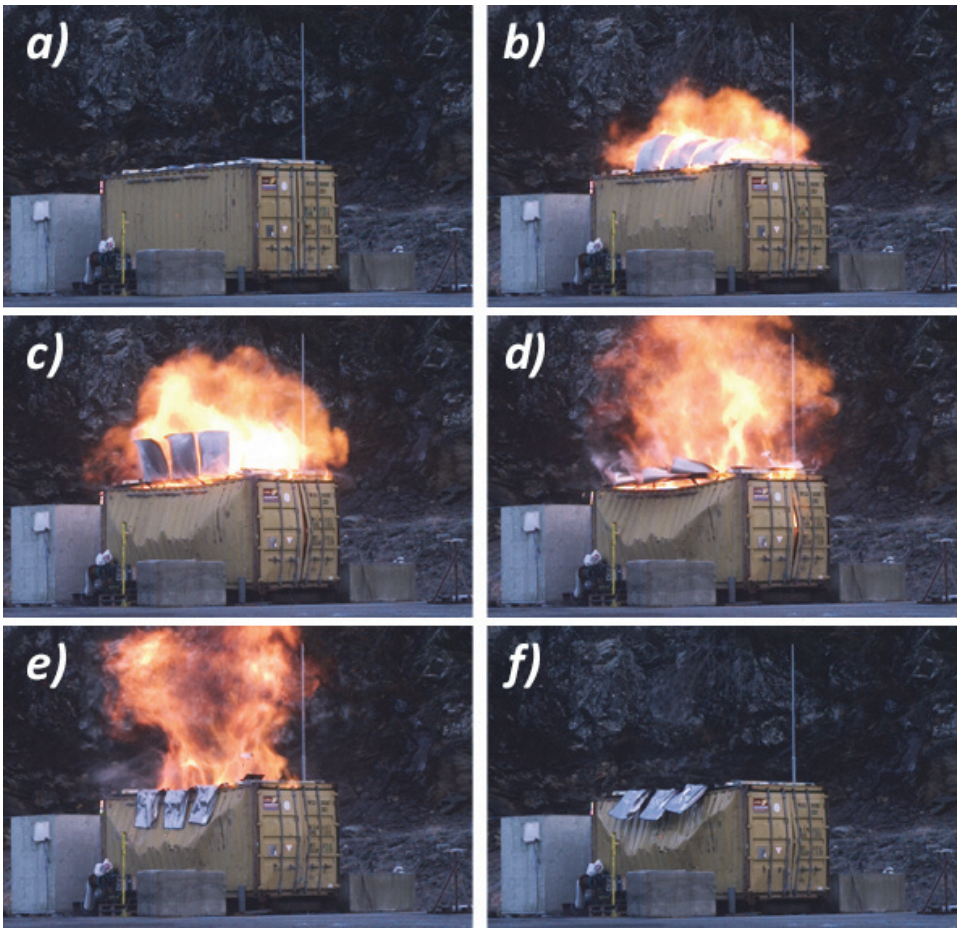

Figure 17: Opening of vent panels for test 61.

5 Model predictions

This chapter summarises the comparison between experimental results and model predictions.

5.1 Release and dispersion

Figure 18 shows experimental and predicted hydrogen concentration profiles at the time of ignition. Several of the model predictions capture the stratification reasonably well, but some do not. For prediction M1a, all monitor points were placed relative to the ground, and not relative to the floor inside the container (i.e. about 0.5 m below the actual measurements). The corrected values (M1b) capture the stratification reasonably well. The results reported for M3 and M6 do not indicate any significant stratification. Insufficient refinement of the grid near the release point explains the results for M6. For prediction M7, the actual CFD simulation (M7a) captures the stratification, but the concentrations are diluted with air from the outside when the simulated cloud is transferred to coarser grids (M7b, M7c and M7d).

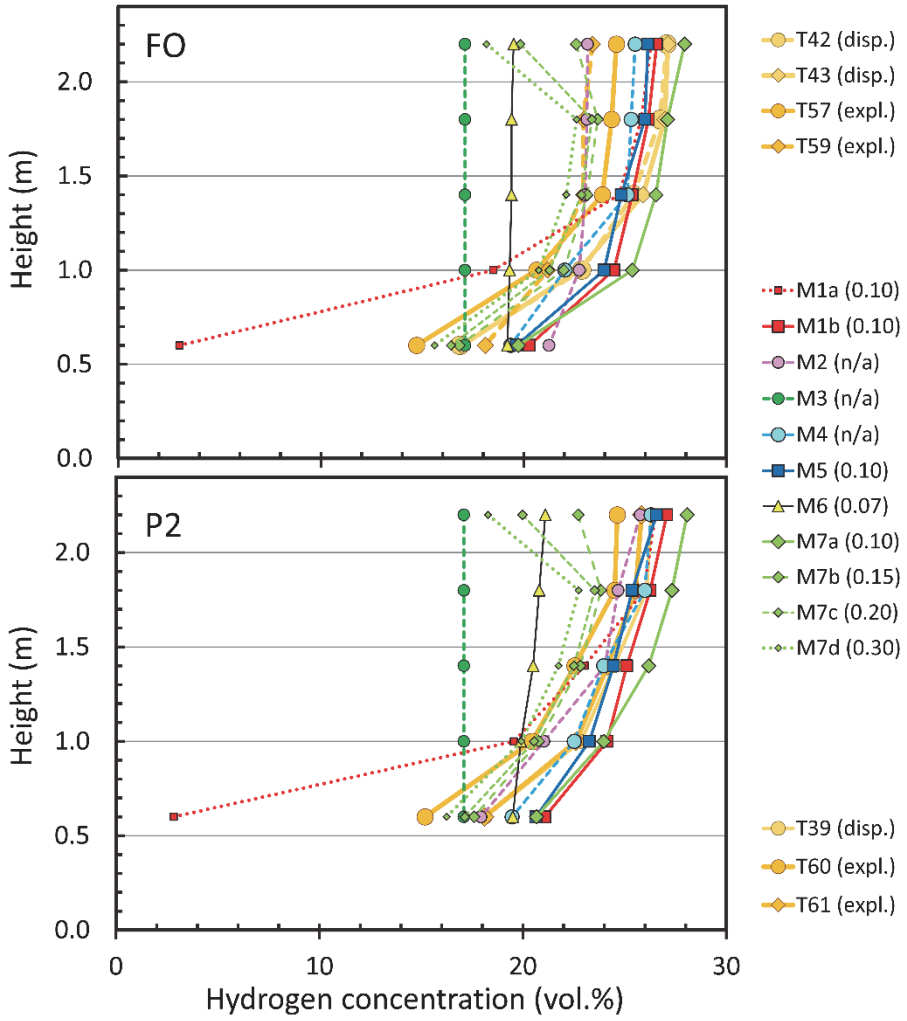

Figure 18: Concentration profiles at time of ignition.

Figure 19 compares model predictions (lines) and experimental results (points) for hydrogen concentration in the positions indicated in Figure 10 for test configurations with frame only (FO) and pipe rack in centre position (P2). The overall results are similar for tests with and without pipe rack. The experimental values indicated for position A4' (FO) in Figure 19 are most erroneous, possibly due to a leak in the sampling tube.

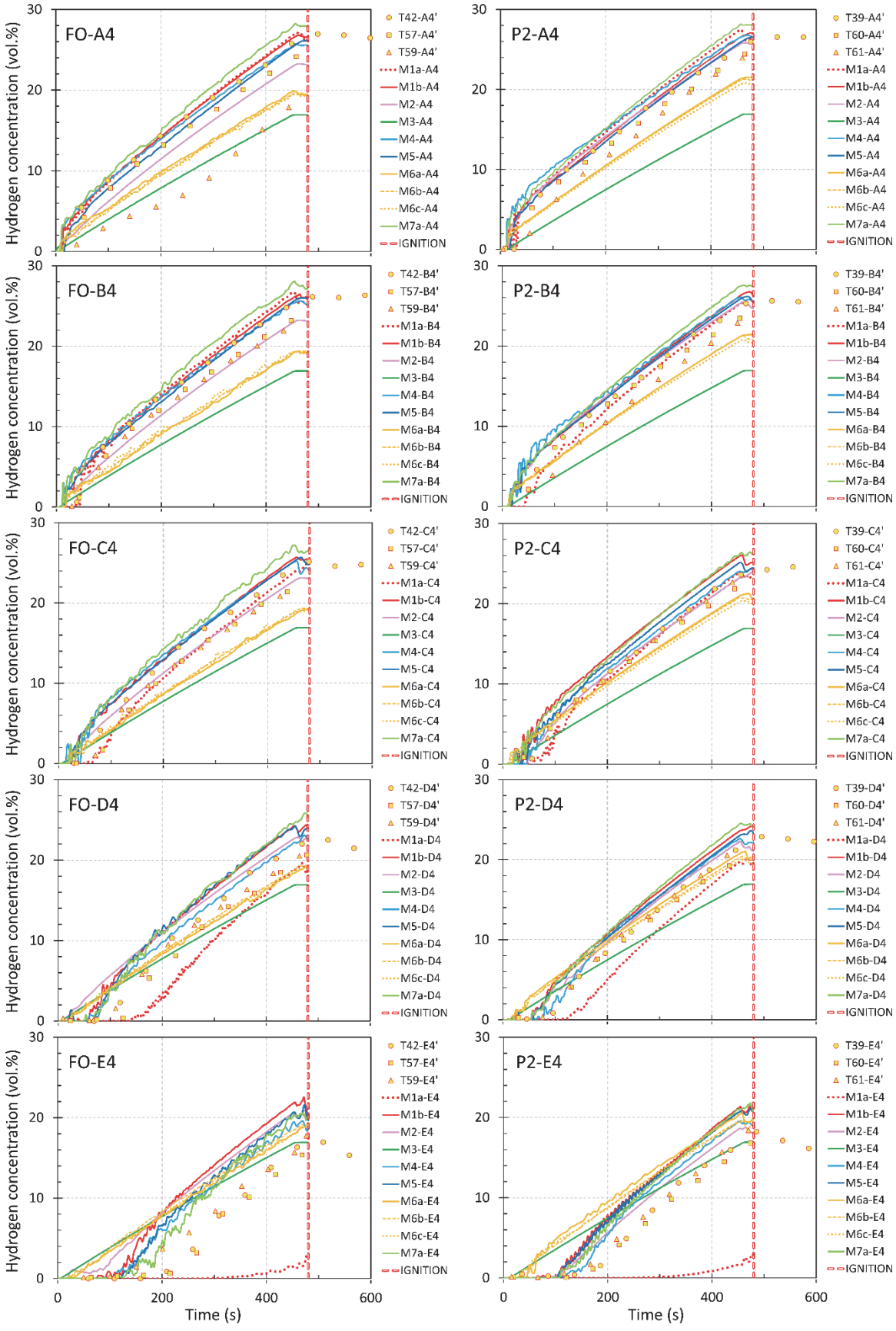

Figure 19: Model predictions for hydrogen dispersion with frame only (FO) and pipe rack (P2).

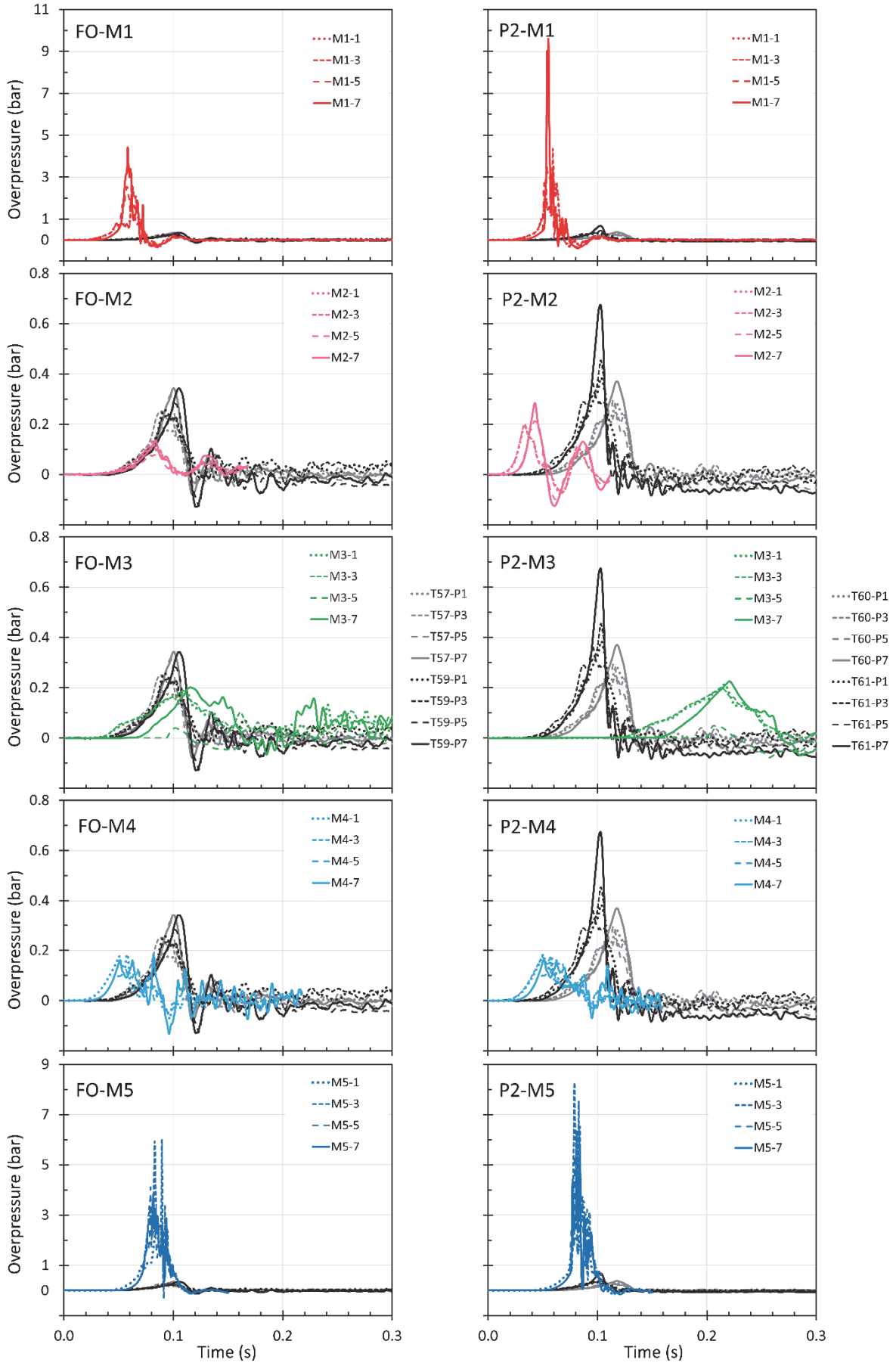

Figure 20: Predicted pressure-time histories for models M1-M5.

5.2 Vented explosions

Figure 20 and Figure 21 compare pressure-time histories from experiments and CFD simulations. In general, predictions M1 and M5-M7, all using the CFD tool FLACS, significantly overpredict the explosion pressure, whereas M2-M4 underpredict.

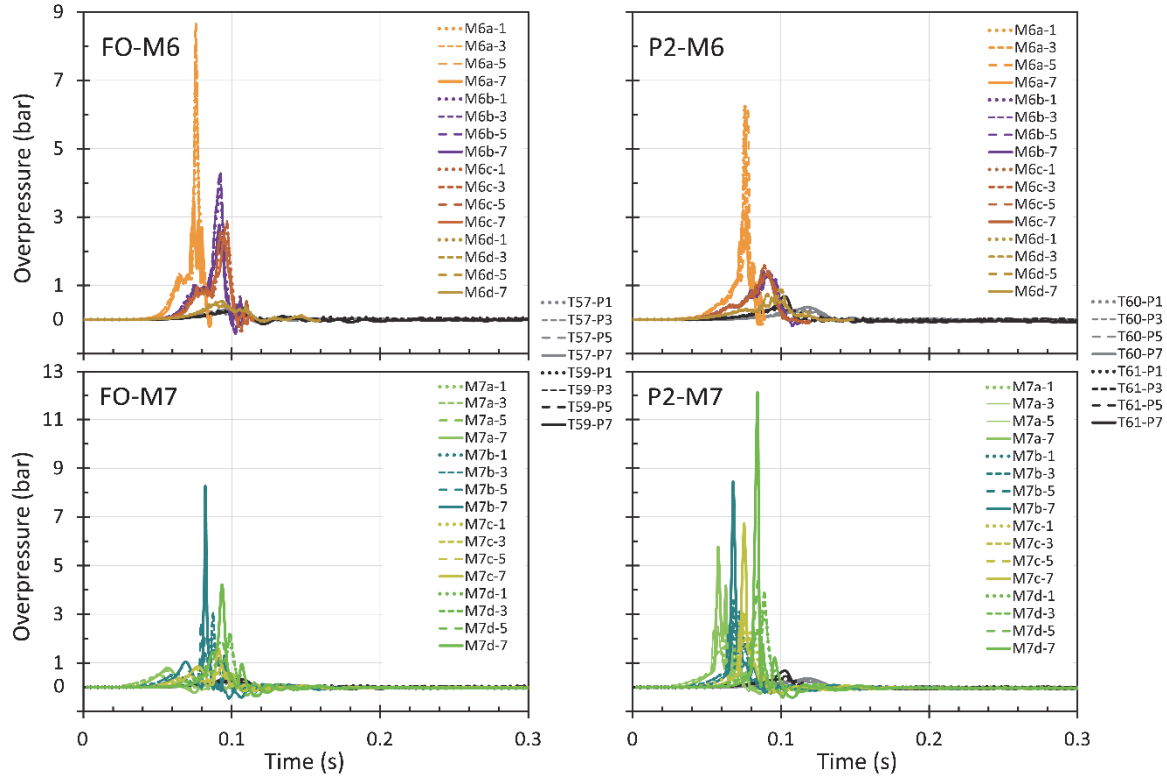

Figure 21: Predicted pressure-time histories for models M6 and M7.

Figure 22 summarises the maximum overpressure and corresponding pressure impulse predicted by the various modellers for both scenarios. The results reported by M6 and M7 reveal significant effect of grid size, including opposite trends with and without the pipe rack (M6).

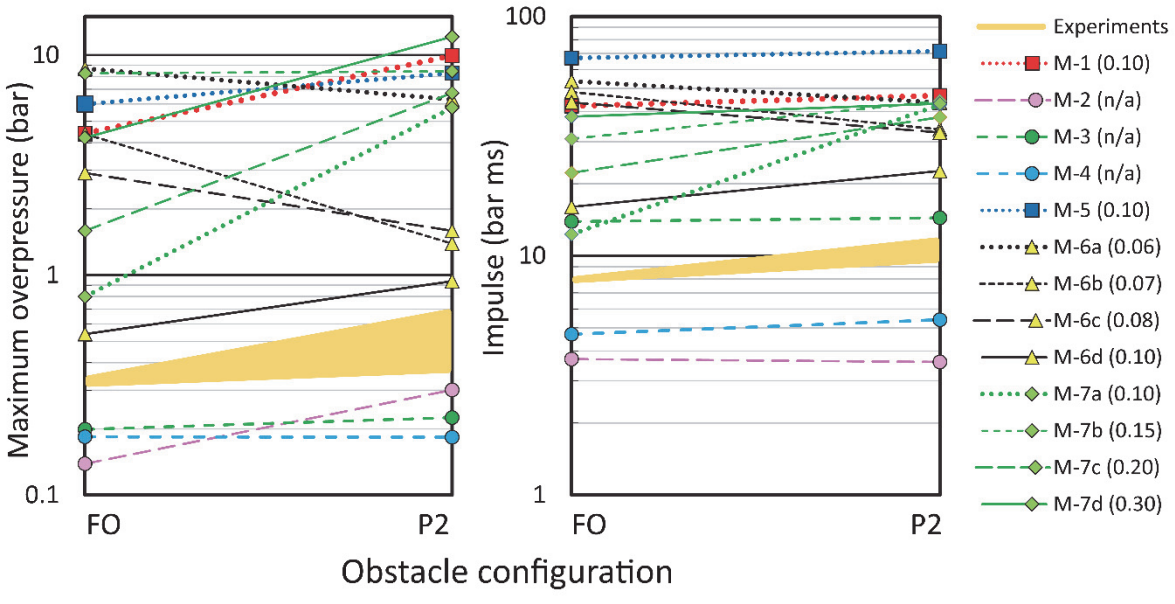

Figure 22: Summary of results for the CFD tools.

Figure 23 summarises the maximum overpressures predicted by the engineering models for both scenarios, assuming various homogeneous hydrogen concentrations inside the container. The results show less variability than the predictions obtained with the CFD tools.

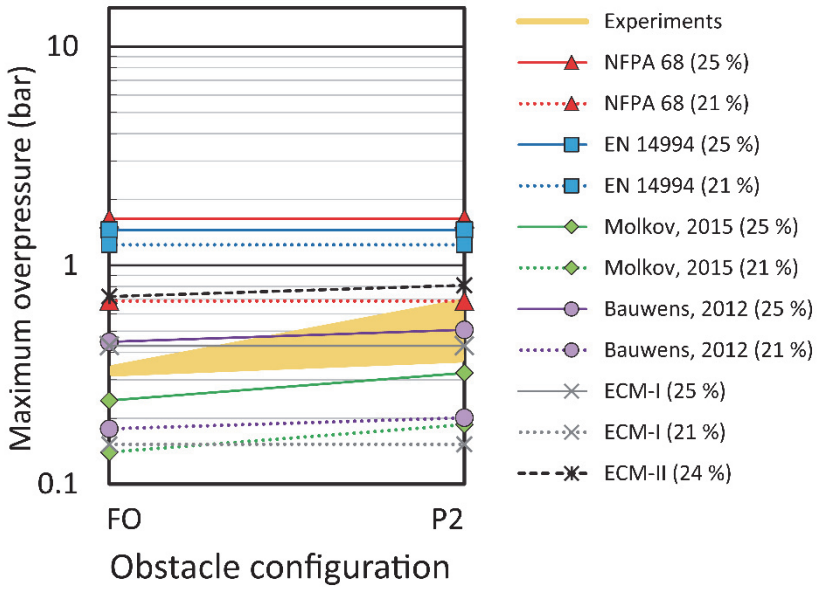

Figure 23: Summary of results for the empirical and phenomenological engineering models.

6 Discussion

The scenarios selected for the second blind-prediction benchmark study in the HySEA project were challenging from a modelling point of view. Long-duration releases from small sources and gradual stratification in large enclosures imply time-consuming CFD simulations. Furthermore, flame propagation in inhomogeneous mixtures and congested geometries, combined with the transient flow and structural dynamics characteristic for vented deflagrations in weak enclosures, are inherently complex phenomena. However, typical application areas for consequence models, such as design optimisation and risk assessments for industrial facilities, may involve a wider range of spatial scales and significantly more complex scenarios. As such, the results from the blind-prediction benchmark exercise provide a realistic measure of the variability that can be expected from this type of engineering calculations.

The concentration measurements summarised in Figure 15 and Figure 18 indicate moderate loss of fuel prior to ignition for tests 57, 59 and 60 and/or somewhat lower mass flow in the releases for test 57 and 59 (Figure 13). This is consistent with the higher explosion pressures and more severe wall deflection measured in test 61, compared to test 60 (Table 2 and Figure 16). This implies that the effect of introducing the pipe rack (P2) may not be as pronounced as indicated in Figure 22 and Figure 23, and that the pressures measured without the pipe rack (FO) probably would have been somewhat higher without loss of fuel.

Figure 18 shows that several modellers predicted the stratification inside the container reasonably well (M1b, M4, M5 and M7a), given the inherent uncertainty in the experimental results (Figure 13 and Figure 15). Several of the deviations between model predictions and experimental results can be explained by user errors, such as misplaced monitor points (M1a), insufficient refinement of the jet release (M6), and inconsistent transformation of results from one computational grid to coarser grid resolutions (M7bcd). This implies that the accuracy of the model predictions can be significantly improved through measures such as automated gridding, improved training, better user documentation and certification of users.

The use of a relatively coarse mesh for the dispersion simulations is the primary explanation for the reduced overall concentration and lack of stratification in the prediction with OpenFOAM (M3 in Figure 18). Limited spatial resolution results in excess diffusion of hydrogen, rapid mixing, and hence very limited stratification (similar to prediction M6). Furthermore, to reduce the simulation time, the computational mesh covered only the interior of the container, and atmospheric boundary conditions were applied for the 20 holes along the walls. This resulted in pressure gradients inside the container during the release, discharge of hydrogen, and lower fuel concentrations.

Significant deviations in the prediction of the concentration field in the flammable cloud will inevitably influence the predictions for the maximum reduced explosion pressure. As such, it is not straightforward to interpret the significant spread in maximum explosion pressure and impulse for model predictions M6 (abcd) and M7 (bcd). Nevertheless, it seems clear that the results from the CFD simulations vary significantly with grid resolution. Since it may not be straightforward to obtain grid convergence for porosity/distributed resistance (PDR) models, such as FLACS, a short-term solution for users of the software may entail updated grid guidelines for scenarios with highly reactive fuels such as hydrogen.

None of the models listed in Table 4 include the effect of the structural response of weak enclosures, such as shipping containers (Table 1). Significant deflections of the walls increase the volume of the container, which may result in lower explosion pressures compared to a rigid structure (Atanga *et al.*, 2018). Figure 17 illustrates how significant deformation of the walls creates additional openings in the container, in particular the gaps between the upper edge of the side walls and the steel frame supporting the vent panels. The severe bulging of the doors also results in a temporary opening. It is not straightforward to predict the effect of the coupling between moving walls and a propagating flame inside the containers on the rate of combustion and pressure build-up inside the enclosures.

According to Table 2, the vent panels opened consistently in all tests. However, Figure 16 reveals that the maximum reduced explosion pressures occurred when the vent panels had opened approximately 45°. This implies that the most critical part of the venting process took place well before the panels were fully open. None of the three models that underpredict the explosion pressure in Figure 22 (M2, M3 and M4) considered the actual opening time and movement of the vent panels. The areas covered by the panels were treated as closed until the internal pressure reached the static opening pressure (0.1 bar), and thereafter as fully open. This modelling approach results in a ‘perfect’ venting device, that hardly can be realised in practice. This is likely to have contributed significantly to the underprediction. The CFD tool FLACS (M1, M5, M6 and M7) includes sub-grid models for various types of venting devices, including hinged panels. However, investigations conducted in the aftermath of the blind-prediction study reveal that the results can be quite sensitive to the representation of the vent panels, including the dynamic response of the panels. Future modelling work should focus on improved representation of realistic explosion venting devices (EN 14797, 2006).

The predictions obtained with the empirical and phenomenological engineering models (Figure 23) show less variation compared to the predictions obtained with various CFD tools (Figure 22). This is hardly surprising, since the geometry of a 20-foot shipping container is relatively simple. The stratification of hydrogen inside the container results in a highly reactive layer beneath the ceiling, and this may limit the effect of the internal obstacle on flame propagation and pressure build-up. There is nevertheless significant potential for improving the performance of empirical and phenomenological engineering models (Lakshmipathy *et al.*, 2018).

The significant spread in predictions from modellers using the same CFD tool demonstrates a need for improved documentation and training of users. The variability can also be reduced by implementing automated and carefully validated procedures for setting up simulations, including the generation of the computational mesh. The significant deviations between model predictions and experiments for the maximum reduced explosion pressure suggest that there is significant potential for improving the models for turbulent reacting flow in the various simulation tools. It is essential for modellers to be aware of the inherent limitations of the model systems they use, and to critically evaluate the model predictions considering available experiments and documented model performance from systematic validation studies (Skjold *et al.*, 2013; Tolias *et al.*, 2018).

7 Conclusions

The second blind-prediction study in the HySEA project explored a two-stage chain of events, starting with release and dispersion of hydrogen inside 20-foot ISO containers, followed by vented deflagrations. Although several modellers predicted the stratification of hydrogen inside the container with reasonable accuracy, the large spread in results for the maximum reduced explosion pressure suggests that the scenarios represented a significant challenge for modellers. It is foreseen that the blind-prediction exercises performed as part of the HySEA project will contribute to increased awareness amongst developers and users of advanced consequence models, as well as model improvements and updated documentation and guidelines.

Acknowledgements

The HySEA project receives funding from the Fuel Cells and Hydrogen 2 Joint Undertaking (FCH 2 JU) under grant agreement No 671461. This Joint Undertaking receives support from the European Union's Horizon 2020 research and innovation programme and United Kingdom, Italy, Belgium and Norway. The members of the HySEA consortium gratefully acknowledge the valuable contributions from the members of the HySEA Advisory Board: Simon Jallais and Elena Vyazmina from Air Liquide, Derek Miller from Air Products, Carl Regis Bauwens from FM Global and Y.F. (John) Khalil from United Technologies Research Center (UTRC).

Disclaimer

A part of this work was co-funded by the Health and Safety Executive (HSE). The contents of the publication, including any opinions and/or conclusions expressed are those of the authors alone and do not necessarily reflect HSE policy. The same applies to the contributions from the other organizations.

References

Atanga, G., Lakshmipathy, S., Skjold, T., Hisken, H. & Hanssen, A.G. (2018). Structural response for vented hydrogen deflagrations: coupling CFD and FE tools. *International Journal of Hydrogen Energy*, DOI: https://doi.org/10.1016/j.ijhydene.2018.08.085

Baraldi, D., Kotchourko, A., Lelyakin, A., Yanez, J., Gavrikov, A., Efimenko, A., Verbecke, F., Makarov, D., Molkov, V. & Teodorczyk, A. (2010). An inter-comparison exercise on CFD model capabilities to simulate hydrogen deflagrations with pressure relief vents. *International Journal of Hydrogen Energy*, 35: 12381-12390.

Baraldi, D., Melideo, D., Kotchourko, A., Ren, K., Yanez, J., Jedicke, O., Giannissi, S.G., Tolias, I.C., Venetsanos, A.G., Keenan, J., Makarov, D., Molkov, V., Slater, S., Verbecke, F. & Duclos, A. (2017). Development of a model evaluation protocol for CFD analysis of hydrogen safety issues the SUSANA project. *International Journal of Hydrogen Energy*, 42: 7633-7643.

Bauwens, C.R. & Dorofeev, S.B. (2014). Effect of initial turbulence on vented explosion overpressures from lean hydrogen–air deflagrations. *International Journal of Hydrogen Energy*, 39: 20509-20515.

Bauwens, C.R., Chaffee, J. & Dorofeev, S.B. (2011). Vented explosion overpressures from combustion of hydrogen and hydrocarbon mixtures. *International Journal of Hydrogen Energy*, 36: 2329-2336.

Bauwens, C.R., Chao, J. & Dorofeev, S.B. (2012). Effect of hydrogen concentration on vented explosion overpressures from lean hydrogen–air deflagrations. *International Journal of Hydrogen Energy*, 37: 17599-17605.

EN 14797 (2006). *Explosion venting devices.* European Committee for Standardization (CEN), Brussels, Belgium: 30 pp.

EN 14994 (2007). *Gas explosion venting protective systems*. European Committee for Standardization (CEN), Brussels, Belgium: 30 pp.

García, J., Baraldi, D., Gallego, E., Beccantini, A., Crespo, A., Hansen, O.R., Høiset, S., Kotchourko, A., Makarov, D., Migoya, E., Molkov, V., Voort, M.M. & Yanez, J. (2010). An intercomparison exercise on the capabilities of CFD models to reproduce a large-scale hydrogen deflagration in open atmosphere. *International Journal of Hydrogen Energy*, 35: 4435-4444.

Gexcon (2018). *FLACS User's Manual v10.6 r3*. Gexcon, Bergen.

Lakshmipathy, S., Skjold, T., Hisken, H. & Atanga, G. (2018). Consequence models for vented hydrogen deflagrations: CFD vs. engineering models. *International Journal of Hydrogen Energy*, DOI: https://doi.org/10.1016/j.ijhydene.2018.08.079

Makarov, D., Verbecke, F., Molkov, V., Roe, O., Skotenne, M., Kotchourko, A., Lelyakin, A., Yanez, J., Hansen, O., Middha, P., Ledin, S., Baraldi, D., Heitsch, M., Efimenko, A. & Gavrikov, A. (2009). An inter-comparison exercise on CFD model capabilities to predict a hydrogen explosion in a simulated vehicle refuelling environment. *International Journal of Hydrogen Energy*, 34: 2800-2814.

Molkov, V. & Bragin, M. (2015). Hydrogen–air deflagrations: Vent sizing correlation for low-strength equipment and buildings. *International Journal of Hydrogen Energy*, 40: 1256-1266.

NFPA 68 (2013). *Standard on explosion protection by deflagration venting*. National Fire Protection Association (NFPA), Quincy, Massachusetts. ISBN 978-145590622-2.

NFPA 68 (2018). *Standard on explosion protection by deflagration venting*. National Fire Protection Association (NFPA), Quincy, Massachusetts. ISBN 978-145591896-6.

Razus, D.M. & Krause, U. (2001). Comparison of empirical and semi-empirical calculation methods for venting of gas explosions. *Fire Safety Journal*, 36: 1-23.

Sinha, A, Rao, M.V.C. & Wen, J. (2018a). Comparison of engineering and CFD model predictions for overpressures in vented explosions. Twelfth International Symposium on Hazards, Prevention and Mitigation of Industrial Explosions (12 ISHPMIE), Kansas City, 12-17 August 2018.

Sinha, A. & Wen, J. (2018). Phenomenological modelling of external cloud formation in vented explosions. Twelfth International Symposium on Hazards, Prevention and Mitigation of Industrial Explosions (12 ISHPMIE), Kansas City, 12-17 August 2018.

Sinha, A., Rao, V.C.M. & Wen, J.X. (2018b). Performance evaluation of empirical models for vented lean hydrogen explosions. *International Journal of Hydrogen Energy*, DOI: https://doi.org/10.1016/j.ijhydene.2018.09.101

Skjold, T. (2018). Vented hydrogen deflagrations in 20-foot ISO containers. Twelfth International Symposium on Hazards, Prevention and Mitigation of Industrial Explosions (12 ISHPMIE), Kansas City, 12-17 August 2018: 24 pp.

Skjold, T., Hisken, H., Lakshmipathy, S., Atanga, G., Carcassi, M., Schiavetti, M., Stewart, J.R., Newton, A., Hoyes, J.R., Tolias, I.C., Venetsanos, A.G., Hansen, O.R., Geng, J., Huser, A., Helland, S., Jambut, R., Ren, K., Kotchourko, A., Jordan, T., Daubech, J., Lecocq, G., Hanssen, A.G., Kumar, C., Krumenacker, L., Jallais, S., Miller, D. & Bauwens, C.R. (2018b). Blind-prediction: estimating the consequences of vented hydrogen deflagrations for homogeneous mixtures in 20-foot ISO containers. *International Journal of Hydrogen Energy*, DOI: https://doi.org/10.1016/j.ijhydene.2018.06.191

Skjold, T., Hisken, H., Lakshmipathy, S., Atanga, G., van Wingerden, M., Olsen, K.L., Holme, M.N., Turøy, N.M., Mykleby, M. & van Wingerden, K. (2018c). Vented hydrogen deflagrations in containers: effect of congestion for homogeneous and inhomogeneous mixtures. *International Journal of Hydrogen Energy*, DOI: https://doi.org/10.1016/j.ijhydene.2018.10.010

Skjold, T., Pedersen, H.H., Bernard, L., Middha, P., Narasimhamurthy, V.D., Landvik, T., Lea, T & Pesch, L. (2013). A matter of life and death: validating, qualifying and documenting models for simulating flow-related accident scenarios in the process industry. *Chemical Engineering Transactions*, 31: 187-192.

Skjold, T., Siccama, D., Hisken, H., Brambilla, A, Middha, P., Groth, K.M. & LaFleur, A.C. (2017). 3D risk management for hydrogen installations. *International Journal of Hydrogen Energy*, 42: 7721-7730.

Skjold, T., Souprayen, C. & Dorofeev, S. (2018a). Perspective: fires and explosions. *Progress in Energy and Combustion Science*, 64: 2-3.

Sommersel, O.K., Bjerketvedt, D, Christensen, S., Krest, O. & Vaagsaether, K. (2008). Application of background oriented Schlieren for quantitative measurements of shock waves from explosions. *Shock Waves*, 18: 291-297.

Sommersel, O.K., Vaagsaether, K. & Bjerketvedt, D. (2017). Hydrogen explosions in 20′ ISO container. *International Journal of Hydrogen Energy*, 42: 7740-7748.

Sustek, J. & Janovsky, B. (2013). Comparison of empirical and semi-empirical equations for vented gas explosion with experimental data. *Journal of Loss Prevention in the Process Industries*, 26: 1549-1557.

Tolias, I.C., Giannissi, S.G., Venetsanos, A.G., Keenan, J., Shentsov, V., Makarov, D., Coldrick, S., Kotchourko, A., Ren, K., Jedicke, O., Melideo, D., Baraldi, D., Slater, S., Duclos, A., Verbecke, F. & Molkov V. (2018). Best practice guidelines in numerical simulations and CFD benchmarking for hydrogen safety applications. *International Journal of Hydrogen Energy*, DOI: https://doi.org/10.1016/j.ijhydene.2018.06.005

Venetsanos, A.G., Papanikolaou, E. & Bartzis, J.G. (2010). The ADREA-HF CFD code for consequence assessment of hydrogen applications. *International Journal of Hydrogen Energy*, 35: 3908-3918.